Sensitivity of Fields within Magnetically Shielded Volumes to Changes in Permeability

T. Andalib[b,*], C.P. Bidinosti[a,b], R.R. Mammei[a,b], J.W. Martin[a,b], A. Bunch of other People[a]

[a] *Physics Department, The University of Winnipeg, 515 Portage Avenue, Winnipeg, MB, R3B 2E9, Canada*
[b] *Department of Physics and Astronomy, University of Manitoba, Winnipeg, MB R3T 2N2, Canada*

Abstract

Future experiments seeking to measure the neutron electric dipole moment (nEDM) require stable and homogeneous magnetic fields. The stability of the magnetic field within a magnetically shielded volume is influenced by a number of factors. In this paper, we study one of these factors, which is the dependence of the internally generated field on the permeability of the material. We also provide measurements of the temperature-dependence of the permeability of the material, and indicate the extrapolation yet required to adequately use these measurements to design future nEDM experiments.

Keywords: Magnetic Shielding, Neutron Electric Dipole Moment, Magnetic Field Stability

1. Introduction

The next generation of neutron electric dipole moment (EDM) experiments aim to measure the EDM d_n with proposed precision $\delta d_n \lesssim 10^{-27}$ e-cm [1, 2, 3, 4, 5, 6, 7, 8, 9]. In the previous best experiment [24], which discovered $d_n < 3 \times 10^{-26}$ e-cm (90% C.L), effects related to magnetic field homogeneity and instability were found to dominate the systematic error. A detailed

*Corresponding author
Email address: andalibt@myumanitoba.ca (T. Andalib)

understanding of passive and active magnetic shielding, magnetic field generation within shielded volumes, and precision magnetometry is expected to be crucial to achieve the systematic error goals for the next generation of experiments. Much of the R&D effort for these experiments is focused on careful design and testing of various magnetic shield geometries with precision magnetometers [11, 12, 13, 14, 15].

The nEDM experiment at TRIUMF aims to determine $\delta d_n \sim 10^{-27}$ e·cm. A DC magnetic field of typically $B_0 = 1$ μT is used to provide the quantization axis for the UCN, normally directed vertically in the apparatus. The experimental cycle involves a Ramsey sequence, where the UCN spins are oriented into the horizontal plane by applying an oscillating horizontal B_1 field, followed by a free precession period, then an additional application of a second B_1 pulse coherent in phase with the first. The UCN are then drained from the measurement cell and the number of UCN in both the spin-up state and spin-down state are counted. By varying the B_1 oscillation frequency, the central resonant frequency may be deduce with high precision. Normally four fills of the measurement cell, with four different B_1 frequencies are used to extract the resonant frequency. In order to extract d_n, the resonant frequency measurement is conducted with an electric field E oriented parallel to the main B_0 field, and then again with E oriented antiparallel to the main B_0 field. A problem in these experiments is if the magnetic field drifts over the course of the measurement period, it worsens the statistical precision with which d_n can be determined. For a $\delta d_n \sim 10^{-27}$ e·cm measurement, the average field over one fill of the measurement cell must be known to the 10 fT level or better (which occurs typically on a timescale of 100 s), and the field is seldom stable to this level. For this reason, experiments use a comagnetometer and/or surrounding atomic magnetometers to correct the magnetic field to this level [**? ? ?**]. In order for this correction technique succeed, gradient fields must be controlled or corrected for at the < 1 nT/m level. Furthermore the stability of the B_0 field must be controlled as well as possible, normally at the 1-10 pT level over the UCN free-precession time.

The B_0 magnetic field generation system for a typical nEDM experiment comprises a coil placed within a passively magnetically shielded volume. The passive magnetic shield is generally composed of a multi-layer shield formed from thin shells of high-permeability metal (mu-metal). The outer layers of this shield are normally cylindrical [**?**] or forming the walls of a magnetically shielded room [27]. The innermost magnetic shield is normally a specially shaped shield, where the design of the coil in relation to shield is carefully taken into account to achieve adequate homogeneity.

The active compensation system will be used to reduce the external

Mechanical and temperature changes of the passive magnetic shielding [29, 26], and the demagnetization procedure [26**?**], affect the stability of the magnetic field within magnetically shielded rooms. Active stabilization of the magnetic field surrounding magnetically shielded rooms can also improve the internal stability [**?** **?**]. In nEDM experiments, care must also be taken to stabilize the current supplied to the B_0 coil [**?**], and the coil must be stabilized mechanically relative to the magnetic shielding as well.

One additional affect, which is the subject of this paper, relates to the fact that the B_0 coil in most nEDM experiments is magnetically coupled to the innermost magnetic shield. If the magnetic properties of the innermost magnetic shield would change as a function of time, it then results in a source of instability of B_0. In the present work, we sought to estimate this effect, and to characterize one possible source of instability: changes the magnetic permeability μ of the material with temperature.

While the senstivity of magnetic alloys to temperature variations has been characterized in the past [16, 22], we sought to make these measurements in regimes closer to the operating parameters relevant to nEDM experiments. For these alloys, it is also known that the magnetic properties are set during the final annealing process [20, 30, 22]. In this spirit we performed our measurements on small witness cylinders that were annealed using the process typically used in setting these properties.

2. Sensitivity of Internally Generated Field to Permeability of the Shield $B_0(\mu)$

2.1. Analytical Calculations in Spherical (and Cylindrical) Geometry

The presence of a coil inside the innermost passive shield turns the shield into a return yoke and it is due to the penetration of the magnetic field flux into the magnetic shield. The ratio of the magnetic field inside the coil in the presence of the magnetic shield to that of the coil in free space is called the reaction factor [**?**]. Normally the reaction factor is larger than unity for spherical and cylindrical geometries. The key issue of interest for this work is the dependence of the reaction factor on μ. This factor can be calculated analytically for spherical and cylindrical geometries [17**?**]. Although the dependence of the reaction factor on μ is rather weak for these geometries, the constraints on B_0 stability are very stringent. Thus a small change in the magnetic properties of the innermost shield can result in an unacceptably large change in B_0.

Fig. 1 shows the central magnetic field B as a function of relative $\mu_r = \mu/\mu_0$ for coil radius 0.53 m inside a magnetic shield with the inner radius of 0.57 m and a thickness of 1.5 mm. The dimensions have been selected to be comparable to the dimensions of the ILL nEDM experiment geometry [10, 21]. For a 10% change in relative μ_r (from 20000 to 22000), the magnetic field changes by 0.7 nT.

2.2. Magnetostatic Simulation Results

Finite-element analysis simulations were conducted to analyze the effect of discretizing the surface current, and to test the geometry dependence of the sensitivity of the experiment to changes in μ. Two axially symmetric simulations were conducted using FEMM [**?**]. In the first simulation, the same spherical geometry was used as for the analytical calculations. However, the surface current was discretized to 50 individual circular wires, inscribed onto a sphere, and equally spaced vertically (i.e. a discrete $\cos\theta$ coil). A square sire profile of side length 1 mm was used. As shown in Fig. 1, this simulation gave good agreement with the analytical calculation.

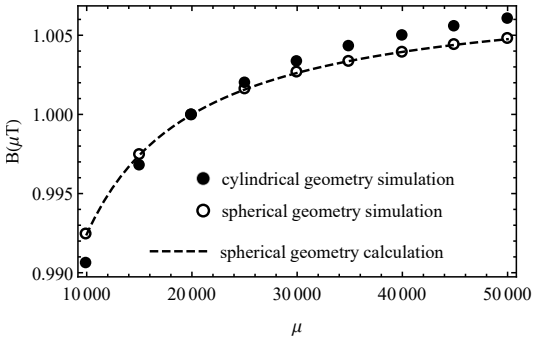

Figure 1: Magnetic field as a function of relative magnetic permeability μ_r for geometries similar to the ILL nEDM experiment. The dashed line is for an ideal spherical surface current of radius 0.53 m inside a spherical shell of inner radius 0.57 m, thickness 1.5 mm. Open and close circles are FEMM-based simulations of spherical and cylindrical geometries with similar dimensions, described in the text. The coil currents have been arranged to give a 1 μT field at the $\mu_r = 20,000$ point.

As an example of one additional axially symmetric geometry, a solenoid within a cylindrical shield was simulated, with equal coil spacings. In the limit of infinite μ, the image currents in the end caps of the shield are an infinite series of coils, giving an ideal infinite solenoid with a uniform field. Again, fifty discrete coils were simulated, where the spacing from an end coil to the inner face of the shield end-cap being half the inter-coil spacing, as appropriate to generate the correct image currents in the infinite μ limit.

As shown in Fig. 1, the slope of $B(\mu)$ is somewhat steeper, and similar in magnitude to the spherical case. We therefore estimate that the scale of the sensitivity of a generic nEDM experiment to global changes in the magnetic permeability is $\frac{\mu}{B}\frac{dB}{d\mu} \sim 0.01$.

In the spherical case the reaction factor is 1.39, meaning that the field generated by the spherical coil is amplified by this multiplicative factor by the presence of the magnetic shield (flux return). In the cylindrical case the reaction factor is 1.35. If the reaction factor is closer to unity, the calculated $\frac{\mu}{B}\frac{dB}{d\mu}$ will be smaller, and the EDM experiment less sensitive to changes in μ.

The results in the two geometries show that there is also a weaker geometry dependence to this statement.

2.2.1. Field within the passive flux return for EDM experiments

For a high-μ innermost shield, the magnetic field lines emanating from the coil all return through the shield. This principle can be used to estimate the magnetic field internal to the material, and in our studies gave good agreement with FEA-based simulations. For the cylindrical geometry described in Sec. 2.2, the B field is largest in the side walls of the cylindrical flux return, attaining a maximum value of 170 μT. For μ_r=20,000 (a typical realistic value for the DC value of μ_r in these shields), the H field is 0.007 A/m. These values are weakly dependent on μ_r. They set a scale for the values of B and H which we sought to replicate in our experiments reported in Section **??**.

2.3. Self-Shielded Coils

A way to decouple the internal coil from the magnetic shield is to design a self-shielded coil [**?** **?**]. In self-shielded coils, the return flux is provided by a second larger coil, rather than through the permeable material of the magnetic shield. In a perfect self-shielded coil, the field at the position of the magnetic shield would be zero, resulting in a reaction factor that is identically unity.

Such coils would completely decouple the properties of the magnetic shield from the homogeneity and stability of the coil itself. Changes in μ of the shield material would then have no impact on the nEDM experiment. Coils incorporating self-shielding in their design are therefore an attractive option for nEDM experiments [**?**].

2.4. Summary of $B_0(\mu)$

For shield-coupled coils, the magnetic field in the region interior to the coil is coupled to the properties of the magnetic shell which is caused by the penetration of the magnetic field flux into the shell material. In a typical nEDM experiment, the sensitivity of the internal magnetic field to changes in μ is

$\frac{\mu}{B}\frac{dB}{d\mu} \sim 0.01$. The coupling can be reduced considerably by using a self-shielded coil design, which does not couple strongly to the innermost magnetic shield.

The field generated in the innermost magnetic shield by a shield-coupled coil is typically $B = 170$ μT, corresponding to $H = 0.007$ A/m. The field in the nEDM measurement volume, as well as in the magnetic shield, must be stable for periods of typically hundreds of seconds (corresponding to frequencies $<<$ 0.01 Hz). This sets the relevant measurement scales for magnetic properties that would be most relevant to nEDM experiment.

3. Measurements of $\mu(T)$

3.1. Previous Measurements and their Relationship to nEDM Experiments

Previous measurements of the temperature dependence of the magnetic properties of high-permeability alloys have been summarized in Refs. [25, 30, 16]. These measurements are normally conducted using a sample of the material to create a toroidal core, where a thin layer of the material is used in order to avoid eddy-current and skin-depth effects [25, 22]. A value of μ is determined by dividing the amplitude of the sensed B-field by the amplitude of the driving AC H-field. The value of μ is then quoted either at or near its maximum attainable value by adjusting H. Depending on the details of the $B - H$ curve for the material in question, this normally means that μ is quoted for H being at or near the coercivity of the material [16, 22], often resulting in large values up to $\mu_r = 4 \times 10^5$.

It is well known that μ measured for toroidal, thin metal wound cores depends on the annealing process used, in particular on the take-out or tempering temperature after the high-temperature portion of the annealing process has been completed [25, 22, 16]. Such studies normally suggest a take-out temperature of 490-500°C. This ensures that the large $\mu_r = 4 \times 10^5$ is furthermore maximal at room temperature. Slight variations around room temperature, and assuming the take-out temperature is not controlled to better than a degree, imply a scale of possible temperature variation of μ of approximately

$\frac{1}{\mu}\frac{d\mu}{dT} \simeq$0.3-1%/K at room temperature would be reasonable to assume [16, 22].

The chief challenge in applying these results to temperature stability of nEDM experiments is that, when used as DC magnetic shielding, the high-permeability alloys are usually operated for significantly different parameters (B, H, and frequencies).

For example, when used in a shielding configuration, the effective permeability is often measured to be typically $\mu_r = 20,000$, in part because the H-field in the material is below the DC coercivity (typically $H_c = 0.4$ A/m [22]). Another example is that, as noted in Section **??**, a more appropriate H for the innermost magnetic shield of an nEDM experiment used as a magnetic flux return for the B_0 coil is 0.007 A/m, again well below the DC coercivity. Furthermore, the innermost magnetic shield of an nEDM experiment is not operated in an AC mode, but rather a DC mode where time (and temperature) stability of the DC B_0 field is the most crucial parameter; i.e. nEDM experiments are typically concerned with slow drifts at < 0.01 Hz timescales whereas the previously reported $\frac{1}{\mu}\frac{d\mu}{dT}$ measurements are cycled at 50 Hz frequencies.

The goal of our experiments was to develop techniques to characterize the material properties of our own magnetic shields post-annealing, in regimes more relevant to nEDM experiments. We created a prototype passive magnetic shield system in support of this (and other) precision magnetic field research for the future nEDM experiment to be conducted at TRIUMF. The shield system is a four-layer mu-metal shield formed from nested right-circular cylindrical shells with endcaps. The inner radius of the innermost shield is 18.44 cm which is equal to its half length. The radii and half-lengths of the progressively larger outer shields increase geometrically by a factor of 1.27. Each cylinder has two end-caps which possess a 7.5 cm diameter central hole. A stove-pipe of length 5.5 cm is place on each hole was designed to minimize leakage of external fields into the progressively shielded inner volumes. The design is similar to another smaller prototype shield discussed in Ref. [**?**]. The magnetic shielding factors of each of the four cylindrical shells, and of various combinations of them, were measured and found to be consistent with $\mu_r \sim 20,000 - 40,000$ for 3.5 μT

applied external axial and transverse fields at frequencies < 0.1 Hz, where the uncertainty in μ_r comes a model uncertainty resulting from incomplete inclusion of the geometry.

In our studies of the material properties of these magnetic shields, two different approaches to measure temperature dependence of μ were pursued. Both approaches involved experiments done using witness cylinders, which are smaller open-ended cylinders (6" in length) made of the same material and annealed at the same time as the prototype magnetic shields. We therefore expect they have the same magnetic properties as the larger prototype shields, and they have the advantage of being smaller and easier to perform measurements with.

The two techniques used were:

1. measuring the axial shielding factor of the witness cylinder as a function of temperature, and
2. measuring the temperature-dependence of the slope of a minor B-H loop, using the witness cylinder as a transformer core, similar to previous measurements of the temperature dependence of μ, but for parameters slightly closer to those encountered in nEDM experiments.

We now discuss the details and results of each technique.

3.2. Axial Shielding Factor Measurements

In these measurements, a witness cylinder was used as a magnetic shield. Small changes in the axial shielding factor are interpreted as a change in the effective μ of the material. This technique is quite different than the usual mutual inductance techniques used by other groups. Our hope was that this geometry would give us more confidence that the properties we were measuring were indeed related to magnetic shielding properties rather than inherent properties of the material.

3.2.1. Magnetic Field Generation

In order to measure the magnetic shielding factor, the witness cylinder was placed within a homogeneous AC magnetic field. The field was created within

the magnetically shielded volume of the prototype magnetic shielding system (described previously in Section **??** in order to provide a good magnetic environment. A short solenoid inside the shielding system was used to produce the magnetic field. The solenoid has 14 turns with 2.6 cm spacing between the wires. The solenoid was designed so that the field produced by the solenoid plus innermost shield approximates that of an infinite solenoid. The magnetic field generated by the solenoid was typically 1 μT. The solenoid current was varied sinusoidally at typically 0.01 to 10 Hz.

3.2.2. Witness cylinder and fluxgate magnetometer

The witness cylinder was placed into this magnetic field generation system as shown schematically in Fig. 2. The cylinder was held in place by a wooden stand.

A Bartington fluxgate magnetometer Mag-03IEL70 (low noise) measured the magnetic field at the center of the witness cylinder. The fluxgate is a "flying lead" model, meaning that each axis is available on the end of a short electrical lead, separable from the other axes. One "flying lead" was placed in the center of the witness cylinder, the axis of the fluxgate being aligned with that of the witness cylinder. The fluxgate was held in place rigidly by a plastic mounting fixture, which was itself mounted to the witness cylinder.

To increase the resolution of the measured signal from the fluxgate, a Bartington Signal Conditioning Unit (SCU) with a low-pass filter set to typically 10-100 Hz and a gain set to typically > 50 was used. The signal from the SCU was demodulated by an SRS830 lock-in amplifier providing the in-phase and out-of-phase components of the signal. (The sinusoidal output of the lock-in amplifier reference output itself was normally used to drive the solenoid generating the magnetic field.) The time constant on the lock-in was typically set to 3 seconds with 12 dB filter.

As shall be described in Section 3.2.5, a concern in the measurement was changes in the field measured by the fluxgate that could arise due from motion of the system components, or other temperature dependences. This could generate

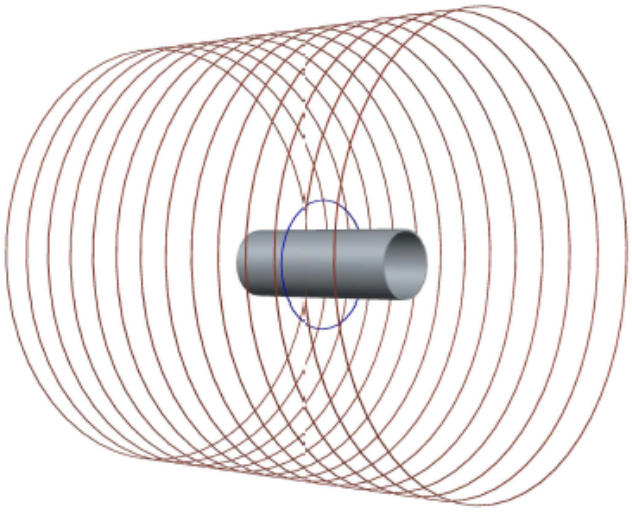

Figure 2: Axial shielding factor measurement setup. The witness cylinder with a radius of 2.54 cm and a length of 15.2 cm is placed inside a solenoid with a radius and a half length of 17.44 cm. The axis of symmetry is along the z-axis. The windings of the solenoid is shown in red. The blue coil with one turn is coupled to the witness cylinder and it has a radius of 5 cm.

a false slope with temperature that might incorrectly be interpreted as a change in the magnetic properties of the witness cylinder.

To address possible motion of the witness cylinder with respect to the field generation system, another coil was wound on a plastic holder mounted rigidly to the witness cylinder. The coil was one loop of copper wire with a radius of 5 cm. The loop coil holder had inner radius of 2.7 cm and an outer radius of about 5 cm. Plastic set screws in the holder fixed the loop coil to be coaxial with the witness cylinder.

Systematic differences in the results from the two coils (the solenoidal coil, and the loop coil) were used to search for motion artifacts. As well, some differences could arise due to the different magnetic field produced by each coil, and so such measurements could reveal a dependence on the profile of the applied magnetic field. In the end, no conclusive difference in the results from either coil could be found. This is described further in Section 3.2.5.

3.2.3. Temperature measurement and data acquisition

The temperature of the witness cylinder was measured by attaching four thermocouples at different points along the outside of the cylinder. To reduce any potential magnetic contamination, T-type thermocouples were used, which have copper and constantan conductors. (K-type thermocouples are magnetic.) Two thermocouples were attached to the edges of the witness cylinder and the other two were attached on opposite sides in the middle. This allowed us to observe the temperature gradient along the witness cylinder.

Thermocouple readings were recorded by a National Instruments NI-9211 temperature input module. The magnetic field (signified by the lock-in amplifier readout) and the temperature were recorded at a rate of 0.2 Hz.

Temperature variations in the experiment were driven by ambient temperature changes in the room, although forced air and other techiques were also tested. These are described further in Section 3.2.5.

3.2.4. Data and Interpretation

An example of the typical data acquired is shown in Fig. 3. For these data, the field applied by the solenoid coil was 1 μT in amplitude, at a frequency of 1 Hz. Fig. 3(a) shows the temperature of the witness cylinder over a four-day measurement. The temperature changes are about 3.5 K and are caused by temperature variations of the laboratory. The shielded magnetic field B within the witness cylinder is anti-correlated with the temperature trend as shown in Fig. 3(b). Here, B is the sum in quadrature of the amplitudes of the in-phase and out-of-phase components. Magnetic field is then interpreted to depend on the temperature, and they are graphed as a function of one another in Fig. 3(c). The slope of Fig. 3(c) has been calculated using a linear fit to the data. The relative slope at 23°C was found to be $\frac{1}{|B|}\frac{d|B|}{dT} \simeq -0.75\%/\mathrm{K}$.

Some deviations from the linear straight-line dependence can be seen in the data. For example, when the temperature changes rapidly, the magnetic field takes some time to respond, resulting in a slope in $B-T$ space that is temporarily different than when the temperature is slowly varying. This is typical of the data that we acquired, that the data would generally follow a straight line if the temperature followed a slow and smooth dependence with time, but the data would not be linear if the temperature varied rapidly or non-monotonically with time.

Another feature of the data was that, on subsequent similar measurements, the value of the slope would not be the same, on a measurement-to-measurement basis, even if very similar experimental parameters were used. A comprehensive set of systematic studies of the factors affecting the slope were performed, and these are presented in Section 3.2.5. A basic summary of those studies was that no external parameter was found that could explain the periodic changes in slope that were observed. Based on these studies, we expect the change in slope is either due to an irreproducibility in the magnetic properties of the material, or due to an uncharacterized systematic error such as a long-time mechanical relaxation of some element of the apparatus.

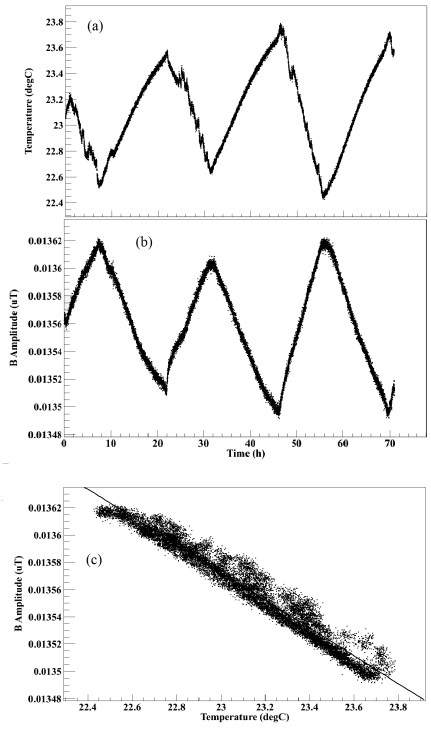

Figure 3: Ambient temperature and shielded magnetic field amplitude, measured over a 70 hour period. (a) temperature of the witness cylinder as a function of time. (b) magnetic field amplitude measured by fluxgate at center of witness cylinder versus time. (c) magnetic field versus temperature. The red line in (c) is a linear fit to data. At 23°C, $\frac{1}{|B|}\frac{d|B|}{dT} = -0.75\%/\mathrm{K}$.

3.2.5. Systematic Studies

Methods of Temperature Variation. In addition to ambient temperature changes, we tried other methods of forced temperature change. In one design, Tygon tubing was wrapped around the witness cylinder in a spiral pattern to flow water whose temperature could be controlled. Mechanical stability issues clearly dominated the systematic uncertainty in that measurement. When water was flowing, the flexibility of the tubing caused a movement in the witness cylinder. The motion was itself temperature-dependent because warmer water caused the tubing to become more supple. To address this effect, the tubes were replaced by copper tubing. But in this case, the challenge was to create enough contact between the tubes and the witness cylinder which was not successful. In another design, a TEC was replaced with the tubing. The main issue with this design was that it did not provide enough cooling for the witness cylinder and also it was creating only local temperature changes on the witness cylinder. In addition, despite of using heat sinks, the heat created by the TEC itself made it very inefficient. We also tried using forced air to heat the witness cylinder. This worked rather well, but the heating had to be done slowly in order to avoid temperature gradients across the apparatus, including the witness cylinder. In the end, using the ambient temperature changes in the room gave the most reproducible results. These followed a relatively stable diurnal cycle with the function of the building's air conditioning system.

Although for most of the measurements the general trend of $B(T)$ graphs was consistent, the shape and positions of the nonlinear parts of $B-T$ graphs were changing. The changes in the B vs. temperature slope always correlate with sharper changes in the temperature with time. The effect is most pronounced when a temperature that is decreasing with time suddenly changes to increasing, or vice-versa. However, we have incorporated the uncertainty from this effect into our stated range of values.

Field profile dependence and mechanical stability. As mentioned earlier, a concern in the measurement was that motion of the witness cylinder, the solenoidal

coil, and the innermost magnetic shield relative to one another could generate a false temperature slope. Another concern was that the spatial variation of the magnetic field generated by the coil could somehow affect the measurement. To address these concerns, a loop coil rigidly mounted to the witness cylinder was used to search for any differences compared to results measured with the solenoidal coil.

The result of this study was that it did not reduce the typical slopes measured, nor improve their reproducibility. In the end, repeated measurements of temperature slopes using the loop coil fell in the range $0.4\%/\mathrm{K} < |\frac{1}{B}\frac{dB}{dT}| < 1.5\%/\mathrm{K}$. Similar measurements for the solenoidal coil yielded $0.3\%/\mathrm{K} < |\frac{1}{B}\frac{dB}{dT}| < 0.8\%/\mathrm{K}$.

In general, the slopes measured with the loop coil are larger than for the solenoidal coil. A partial explanation of this difference is offered by the field profile generated by each coil, and its interaction with the witness cylinder. This is addressed further in Section 3.2.6.

However, the range of slopes measured in different trials still varied within the stated ranges. We conclude that whatever is causing the slopes to change periodically is likely unrelated to motion of the witness cylinder relative to the magnetic elements in the system.

Other potential motion artifacts due to thermal expansion of components was also considered. The thermal expansion coefficient of mu-metal is $\sim$10 ppm/K [22]. However if the witness cylinder expands uniformly in both thickness and radius, the shielding factor is to first order unchanged. In general, even unnatural asymmetric and twisting motions of the fluxgate sensor and witness cylinder tended to generate temperature slopes in the magnetic field at the level < 30 ppm/K. The general homogeneity of the magnetic field at the fluxgate sensor position and of the applied magnetic field within which the witness cylinder was placed aided in minimizing motion artifacts.

As the witness cylinder was put through its diurnal heating and cooling cycles, so too was the magnetic shield within which the apparatus was placed. Since this magnetic shield is used as a flux return, especially for the solenoidal coil, a concern could be that the measurement confounds temperature depen-

dence of the flux return with the temperature dependence of the shielding factor of the solenoid. We want to clarify that this cannot be the case: any change in μ of the flux return will have an exceedingly small effect on the field produced by the solenoid. This is perhaps best demonstrated by Fig. 1, where the reaction factor in a similar cylindrical geometry is graphed as a function of μ. Based on our measurements, this limits systematic errors from such an effect to be < 200 ppm/K.

The magnetization of the witness cylinder changes the magnetic permeability of the material and so the shielding factor changes. Our studies of degaussing the witness cylinder were consistent with studies that we will report in Section **??**. Essentially, if the shields were degaussed, or if they were left for long periods of time in the small AC field generated by the solenoid, the results for temperature dependences were similar. Improper degaussing procedures were found to induce long-term drifts in the measurement, uncorrelated with temperature. We do not include such data when quoting our measurements of temperature slopes. We do think that part of the range of slopes that we measured is due to the magnetic properties of the material, and that it is possible that some of this range is yet due to insufficient degaussing on our part. This is something we plan to improve in planned future experiments on DC field stability.

Temperature slopes of various components of the apparatus. The temperature coefficients of various components that could affect the measurement were also considered.

The Mag-03IEL70 Bartington magnetic field sensor has a scaling temperature coefficient of 15 ppm/K [**?**]. There is also temperature coefficient for the offset of these sensors, but this is irrelevant for this measurement because of the AC fields and demodulation technique used.

The SRS830 lock-in amplifier has 50 ppm/K amplitude stability [31]. To further test this, the lock-in amplifier was connected to the coil through a 1 Ω resistor with small temperature coefficient. The voltage across the resistor was measured with the lock-in amplifier itself. Any change would then be interpreted

as a change in the current supplied to the coil by the lock-in amplifier. The measured temperature dependence was always $< 0.1\%$/K.

The stability of the system was also tested by replacing the mu-metal witness cylinder with a copper cylinder of very similar dimensions. All other components of the system were the same. The apparatus was then run through its usual experimental cycle over several days. For all such measurements the temperature dependence of the demodulated magnetic was $< 0.1\%$/K. This kind of measurement is unable to address all possible systematic uncertainties. For example, if moving the mu-metal witness cylinder due to some thermal expansion would change the field at the site of the fluxgate, moving the copper cylinder will not make the same change. Nonetheless it is an encouraging result that the system does not measure a strong temperature dependence of the magnetic field when no mu-metal witness cylinder is present. The magnitude of the magnetic field measured at the fluxgate sensor was larger during these measurements because of the lack of magnetic shielding from the copper. So, in some tests the magnetic field generated by the reference channel of the lock-in amplifier was reduced to search for any problems arising from smaller fluxgate signals. No difference was seen within the upper bound stated above.

Different Witness Cylinders. The manufacturer of our prototype magnetic shields provided us with three witness cylinders. All three were used in these measurements. Different cylinders possessed systematically different temperature slopes, although always within the ranges quoted above. These changes are believed to arise from the manufacturing and annealing process. It is known that the take-out temperature in the annealing process has a strong effect on the temperature slopes measured at 50 Hz [**?**].

3.2.6. Geometry correction and determination of $\mu(T)$

To relate the data on $B(T)$ to $\mu(T)$, the shielding factor of the witness cylinder as a function of μ must be known. Finite element simulations in FEMM and OPERA were performed to determine this factor. The simulations are also

useful for determining the effective values of B and H in the material (sometimes called the "demagnetization factor" in the literature), which will be useful to compare to the case for typical nEDM experiments when the innermost shield is used as a flux return.

From the simulations the ratio $\frac{\mu}{B}\frac{dB}{d\mu}$ was calculated. A linear model of the material was used where $\mathbf{B} = \mu\mathbf{H}$ and μ is a constant independent of $\mathbf{H}$. The term $\frac{\mu}{B}\frac{dB}{d\mu} \neq 1$ because the witness cylinders are open ended, and hence even for very large $\mu \to \infty$ the shielding factor asymptotically approaches a constant rather than infinity.

The simulations differed slightly in their results, dependent on whether OPERA or FEMM was used, and whether the solenoidal coil or loop coil were used. Based on the simulations, the result is $\frac{\mu}{B}\frac{dB}{d\mu} = 0.42-0.50$ for the solenoidal coil, with the lower value being given by FEMM and the upper value being given by a 3D OPERA simulation, for identical geometries. This is somewhat lower than the value suggested by Paperno [32] in his fits to simulations performed in OPERA, which we estimate to be 0.6. We adopt our value since it is difficult to determine precisely from Ref. [32]. For the loop coil, we determine $\frac{\mu}{B}\frac{dB}{d\mu} = 0.56-0.65$, the range being given again by a difference between FEMM and OPERA.

Combining the measurement and the simulations, the temperature dependence of the effective μ (at $\mu = 20000$, which is consistent with our measurements) can be calculated by

$$\frac{1}{\mu}\frac{d\mu}{dT} = -\frac{\frac{1}{B}\frac{dB}{dT}}{\frac{\mu}{B}\frac{dB}{d\mu}}. \tag{1}$$

The results of the simulations and measurements are presented in Table 1.

Combining the loop coil and solenoidal coil results, we find $0.6\%/\mathrm{K} \lesssim \frac{1}{\mu}\frac{d\mu}{dT} \lesssim 2.7\%/\mathrm{K}$ to be a reasonable range for the possible temperature slope of μ.

As stated earlier, the simulations also provided a way to determine the typical B and H internal to the material of the witness cylinder. According to the simulations, the B amplitude was typically XXX and the H amplitude was typically XXX. These are somewhat larger than the values normally encountered

	$\lvert\frac{\mu}{B}\frac{dB}{d\mu}\rvert$	$\lvert\frac{1}{B}\frac{dB}{dT}\rvert$ (%/K)	$\frac{1}{\mu}\frac{d\mu}{dT}$ (%/K)
Solenoidal Coil	0.42-0.50	0.3-0.8	0.6-1.9
Loop Coil	0.56-0.65	0.4-1.5	0.6-2.7

Table 1: Summary of OPERA and FEMM simulations and shielding factor measurements, resulting in extracted temperature slopes of μ.

in nEDM experiments, when the innermost shield is used as a flux return.

Furthermore, we remind the reader that the measurements were conducted using AC fields at typically 1 Hz, as opposed to the DC fields normally used in nEDM experiments.

3.3. Transformer Core Measurements

As an alternate method of measuring changes in μ, a method similar to the standard method of magnetic materials characterization via magnetic induction was used. In this measurement technique, the witness cylinder was used as the core of a transformer. Two coils (primary and secondary) were wound on the witness cylinder using multistranded 20-gauge copper wire. The windings were made as tight as possible, but not so tight as to potentially stress the material. The windings were not potted in place.

Each of the three witness cylinders was tested. Data were acquired using different numbers of turns on both the primary and secondary coils (from six to 48 on the primary, and from 7 to 24 on the secondary).

The primary coil generated an AC magnetic field $H(t)$, while the secondary coil was used to measure the EMF induced by the time-varying magnetic flux and hence being proportional to $dB(t)/dt$. To a good approximation

$$H(t) = fracN_pI(t)2\pi R \tag{2}$$

where N_p is the number of turns in the primary, $I(t)$ is the current in the primary, and R is the radius of the witness cylinder, and

$$\frac{dB(t)}{dt} = \frac{V(t)}{t\ell} \tag{3}$$

where $V(t)$ is the voltage generated in the secondary, and t and ℓ are the thickness and length of the witness cylinder.

For a sinusoidal drive current $I(t)$, and under the assumption that $B(t) = \mu H(t)$ with μ being a constant, the voltage generated in the secondary $V(t)$ should be sinusoidal and out of phase with the primary current.

The internal oscillator of a SRS830 lock-in amplifier was used to generate $I(t)$. This was monitored by measuring the voltage across a 1 Ω resistor with small temperature coefficient in the primary loop. The lock-in amplifier was then used to demodulate $V(t)$ into its in-phase X and out-of-phase Y components. The experiment was done at 1 Hz and as small as possible $H(t)$, typically 0.1 A/m in amplitude, to measure the slope of the minor $B - H$ loops near the origin of the $B - H$ space.

The temperature of the core was measured at the same time as the sense voltage using non-magnetic type T thermocouples. Measurements of Y as a function of temperature would then signify a change in μ with temperature. In general, we used ambient temperature variations, as for our axial shielding factor measurements.

The naive expectation is that the out-of-phase Y component should signify a non-zero μ, wherease the in-phase X component should be zero. In practice, due to a combination of saturation, hysteresis, eddy-current losses, and skin-depth effects, the X component is never zero.

It was found experimentally that the amplitude of $H(t)$ had to be kept small compared to the coercivity ($\sim$ 3 A/m) in order to ensure that the Y component was larger than the X component. This is displayed graphically in Fig. 4, where the dependence of Y and X on the amplitude of the applied $H(t)$ is displayed, for a driving frequency of 1 Hz are shown. Clearly the value of X can be considerable compared to Y, for larger H amplitudes near the coercivity. At large amplitudes, the material goes into saturation, and both Y and X eventually decrease at amplitudes much greater than the coercivity. This behavior, and signal-to-noise considerations, drove our decision to measure at typically 0.1 A/m amplitude and 1 Hz.

The observation of nonzero X signal is due to effects such as hysteresis, saturation, eddy currents, and skin depth. Therefore, it is not truly possible to embody the results as a single parameter μ, although we desired to express our results as such. To understand the behavior in Fig. 4 effects, a theoretical model of the hysteresis based on Jiles [23] was used.

The key parameters of Jiles' model are saturation magnetization M_s, mean field parameter α which represents interdomain coupling, a with the dimensions of magnetic field which characterizes the shape of anhysteretic magnetization, bulk magnetization M and the magnetic field H. We adjusted these parameters based on our separate measurements of $B-H$ loops including the initial magnetization curve. These measurements were done at frequencies from 0.01 to 10 Hz. It was found that the frequency dependence predicted by Ref. [23] gave relatively good agreement with the measured B-H loops once the five original (Jiles-Atherton [**?**]) parameters were tuned. These same parameters were then used to model the measurement presented in Fig. 4, including the lock-in amplifier function. As shown in Fig. 4, trends in the measurements and simulations are fairly consistent. The sign of X relative to Y is also correctly predicted by the model (we have adjusted them both to be positive, for graphing purposes). We think that with further tuning of the model, even better agreement could be gotten.

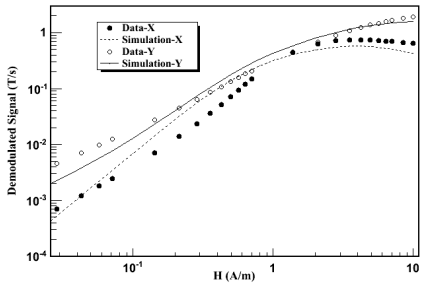

Figure 4: These graphs represent the sense voltage as a function of applied H field at 1 Hz. Graph (a) shows the out-of-phase component X of the measured sense voltage as well as the simulation. Graph (b) shows the in-phase component Y of the signal and its simulation.

The Y and X signals are therefore reminiscent of a complicated set of parameters embodying hysteresis and other losses in the sample. This draws into question the practice of using $Y(T)$ as an indication of the temperature dependence of the magnetic permeability $\mu(T)$.

We nonetheless took data on $Y(T)$ which we naively interpret as $\mu(T)$. We assign no additional systematic error for this simplification, and all our results are subject to this caveat. We comment further that in our measurements of the axial shielding factor, the same caveat exists. In that case one would expect the in-phase X component to dominate the demodulated fluxgate signal. While it does dominate, the Y component is never exactly zero. In a sense, measuring $\mu(T)$ itself is always an approximation, since it is actually the parameters of minor loops in a hysteresis curve which are measured. Our results may be interpreted as a measure of the temperature-dependence of the slopes of those minor loops.

Graphs of $\frac{1}{Y}\frac{dY}{dT}$ as a function of T were made. In general, the data mimicked the behavior of the axial shielding factor measurements, giving a similar level of linearity with temperature as the data displayed in Fig. **??**. Other similar behaviors to those measurement were also observed, for example: (a) when the temperature slope changed sign, Y would temporarily give a different slope with temperature, (b) the overall slope of $1/YdY/dT$ depended on a variety of factors, most notably a dependence on which of the three witness cylinders was used for the measurement, and on differences between subsequent measurements using the same cylinder.

Based on a number of measurements with different cores and windings, the data showed a range of 0.1%/K to 2.1%/K for $\frac{1}{\mu}\frac{d\mu}{dT} = \frac{1}{Y}\frac{dY}{dT}$, again naively assuming the material to be linear as discussed above. The sign of the slope with temperature was the same as the axial shielding factor technique.

We discuss further systematic errors affecting the measurement in the next section.

3.3.1. Systematic Errors

The dominant source of variation between results in this method arose from properties inherent to each witness cylinder. One of the cylinders gave temperature slopes consistently larger $\frac{1}{Y}\frac{dY}{dT} \sim 1.2 - 2.1\%/\mathrm{K}$ than the other two $\frac{1}{Y}\frac{dY}{dT} \sim 0.1 - 0.7\%/\mathrm{K}$. We expect this indicates some difference in the annealing process or subsequent treatment of this cylinder, although to our knowledge the treatment was controlled the same as for the other two cylinders.

Since our goal is to provide input to future EDM experiments on the likely scale of the temperature dependence of μ that they can expect, we phrase our result as a range covering all these results.

In this method the secondary voltage $V(t)$ was measured directly by a lock-in amplifier and so systematics correlated to fluxgate were removed, compared with the axial shielding factor measurement. This method therefore addresses possible systematic drifts in fluxgate performance. It is clear that these were unlikely to dominate the errors in the axial shielding factor measurements.

A possible systematic effect arises due to settling or slight motions of the wires used to wind the primary and secondary coils on the witness cylinders. The coils were wound by hand directly onto the witness cylinder and were held in place by tension. In shorter time measurements when the temperature was not changing, the Y and X values generally did not change at the $< 0.1\%$ level. We do not assign any additional systematic error for possible motion of the windings.

Detailed measurements of the effect of degaussing were conducted for this geometry. In fact, the ability to degauss led us ultimately to select a larger number of primary turns (48) so that we could fully saturate the core using only the lock-in amplifier reference output as a current source.

A computer program was used to control the lock-in amplifier in order to implement degaussing. A sine wave with the measurement frequency (typically 1 Hz) was applied at the maximum lock-in output power. Over the course of several thousand oscillations, the amplitude was decreased linearly to the

measurement amplitude ($\sim$ 0.1 A/m). A possible limitation of this system is that the lock-in amplifier could only be programmed to change its amplitude at the level of 12 bits of precision; we did not study the effect of this in further detail.

An immediately obvious effect was that the Y and X values after degaussing were normally larger than prior to degaussing. We interpret this difference as an increase in the effective μ.

The temperature dependence of Y (and effective μ) did not change significantly. Poor degaussing (for example, degaussing with too few cycles, or ramping too rapidly to zero) could result significantly different initial slopes with temperature, where the effective μ would drift for several hours after degaussing. But after improving the system to have a large number of cycles (consistent with the recommendations of Refs. [26]) the results became consistent with being affected by temperature changes, and were also consistent with previous measurements were no degaussing was done.

To check the stability of the applied current in the primary coil, voltage across a 1 Ω temperature controlled resistor in series with the primary coil was demodulated using a second lock-in amplifier. The result showed $< 0.1\%$/K changes in current ruling out this as an additional source of systematic error.

To reduce the background noise and thermally isolate the witness cylinder, most measurements were done by placing the witness cylinder inside the prototype passive shield. The results did not show a significant change whether they were done with the caps of the prototype passive shield on or off. The results were even consistent when done outside the passive shields.

To summarize, the dominant systematic effects arose due to different similarly prepared cores giving different results, and due to variations in the measured slopes in multiple measurements on the same core. The second of these is essentially the same error encountered in our axial shielding factor measurements. We expect it has the same source; it is likely due to some property of the material the cores are made of, or an additional unknown systematic uncertainty.

Finally we note the primary caveat to these measurements, discussed above, which is that both measurements (transformer core and axial shielding factor) do not truly measure μ. Rather they measure observables related to the slope of minor hysteresis loops in B-H space. They would be more appropriately described by a model like that of Jiles [23], but to extract the temperature dependence of the five parameters of the model is beyond the scope of this work. Instead we acknowledge this fact and relate the temperature dependence of the effective μ measured by each experiment.

We think it is interesting and useful information that the two experiments measure the same scale and sign of the temperature dependence of their respective effective μ's. We feel this is the principal contribution of this work.

3.4. Summary of $\mu(T)$

Each measurement (axial shielding factor measurement, or transformer core measurement) is of the temperature dependence of an effective μ, done in an AC mode at a particular driving amplitude of $H(t)$.

In the axial shielding factor case, we found $0.6\%/\mathrm{K} \lesssim \frac{1}{\mu}\frac{d\mu}{dT} \lesssim 2.7\%/\mathrm{K}$, with the measurement being conducted with a typical H-amplitude of 0.0001-0.001 A/m and at a frequency of 1 Hz. In the transformer core case, we found $0.1\%/\mathrm{K} \lesssim \frac{1}{\mu}\frac{d\mu}{dT} \lesssim 2.1\%/\mathrm{K}$, with the measurement being conducted with a typical H-amplitude of 0.1 A/m and at a frequency of 1 Hz.

Our desire is to provide information relevant to EDM experiments where the coil would couple to innermost magnetic shield in the experiment. We think it would be reasonable to assume that for the parameters relevant to EDM experiments (H of 0-0.007 A/m and frequencies < 0.01 Hz), the temperature dependence of the effective permeability could be of similar scale to these measurements i.e. $\frac{1}{\mu}\frac{d\mu}{dT}$ ranging from 0.1 to 2.7%/K.

4. Summary and Conclusions

Neutron EDM experiments are typically designed with the DC coil being magnetically coupled to the innermost magnetic shield. If the magnetic perme-

ability of the shield changes, this results in a change in the field in the measurement region by an amount $\frac{\mu}{B}\frac{dB}{d\mu} \sim 0.01$. Temperature changes could result in such changes, and it is those temperature changes we sought to constrain by measurement.

The temperature dependence of μ has been measured by two different techniques using open-ended mu-metal cylinders with 6 inches in length. We summarize the overall result as 0.1%/K< $\frac{1}{\mu}\frac{d\mu}{dT}$ <2.7%/K, where the range is driven in part by material properties of the different mu-metal cylinders, and in part by fluctuations measured in the temperature slopes in each measurement.

We provide this range with the following caveats:

- The measurement techniques rely on considerably larger frequencies and H-fields than those relevant to typical nEDM experiments. For frequency, both techniques typically used a 1 Hz AC field, whereas for nEDM experiments the field is DC and stable at the 0.01 Hz level. Furthermore, in one measurement technique the amplitude of H was ~ 0.001 A/m and in the other was ~ 0.1 A/m, while for nEDM experiments $H \sim 0 - 0.007$ A/m and is DC.

- Both measurement techniques extract an effective μ that describes the slope of minor loops in B-H space. A more correct treatment would include a more comprehensive accounting of hysteresis in the material, which is beyond the scope of this work.

Assuming our measurement of 0.1%/K< $\frac{1}{\mu}\frac{d\mu}{dT}$ <2.7%/K and the generic EDM experiment sensitivity of $\frac{\mu}{B}\frac{dB}{d\mu} \sim 0.01$ results in a temperature dependence of the magnetic field in a typical EDM experiment of $\frac{dB}{dT} = 10 - 270$ pT/K. To achieve a goal $\sim pT$ stability in the internal field for EDM experiments, the temperature of the innermost magnetic shield in the EDM experiment should then be controlled to 0.1-0.004 K level. This could be a serious problem for future nEDM experiments. The dependence could be reduced significantly by using self-shielded coils in the EDM experiment, which would reduce the coupling to the innermost magnetic shield.

References

[1] S. N. Balashov *et al.*, arXiv:0709.2428.

[2] A. P. Serebrov *et al.*, JETP Lett. **99**, 4 (2014).

[3] A. P. Serebrov *et al.*, Physics Procedia **17**, 251 (2011).

[4] K. Kirch, AIP Conf. Proc., Vol. 1560, pp. 90-94 (2013).

[5] C. A. Baker, *et al.*, Physics Procedia **17**, 159 (2011).

[6] Y. Masuda, K. Asahi, K. Hatanaka, S.-C. Jeong, S. Kawasaki, R. Matsumiya, K. Matsuta, M. Mihara, and Y. Watanabe, Phys. Lett. A **376**, 1347 (2012).

[7] I. Altarev, *et al.*, Nuovo Cim. C **35**, 122 (2012).

[8] R. Golub and S. K. Lamoreaux, Phys. Rept. **237**, 1 (1994).

[9] T. M. Ito (the nEDM collaboration), J. Phys. Conf. Ser. **69** 012037, 2007.

[10] C. A. Baker, *et al.*, Phys. Rev. Lett. **97**, 131801 (2006).

[11] T. Bryś, *et al.*, Nucl. Instrum. Meth. A **554**, 527 (2005).

[12] S. Afach, *et al.*, J. Appl. Phys. 116, 084510 (2014).

[13] I. Altarev, *et al.* Rev. Sci. Instrum. **85**, 075106 (2014).

[14] M. Sturm, Masterarbeit, T.U. Muenchen (2013).

[15] B. Patton, E. Zhivun, D. C. Hovde, and D. Budker, Phys. Rev. Lett. 113, 013001 (2014).

[16] G. Couderchon, J. F. Tiers, J. Magn. Magn. Mat. 26(1):196-214 (1982).

[17] C. P. Bidinosti *et al.*, AIP Advances 4, 047135 (2014).

[18] W. R. Smythe, McGraw Hill (1950).

[19] V. C. A. Ferraro, Athalone Press (1967).

[20] Kiran Gupta, K. K. Raina, S. K. Sinha, J. Alloys Compd, 429(1):357-364 (2007).

[21] A. Knecht, Dissertation, UZH Zurich (2009).

[22] KruppVDM Magnifer 7904, MDS no. 9004 (2000).

[23] D. C. Jiles, D. L. Atherton, J. Magn. Magn. Mat. 61(1-2):48-60, (1986).

[24] J. M. Pendlebury *et al.*, Phys. Rev. D 92, 092003 (2015).

[25] F. Pfeifer, C. Radeloff, J. Magn. Magn. Mat. 19 (1980) 190-207.

[26] F. Thiel *et al.*, Rev. Sci. Instrum. 78, 035106 (2007).

[27] I. Altarev *et al.*,Rev. Sci. Instrum. 85, 075106 (2014).

[28] I. Altarev *et al.*, J. Appl. Phys. 117, 233903 (2015).

[29] J. Voigt *et al.*, Metrol. Meas. Syst. 20, 239 (2013).

[30] R. M. Bozorth, Ferromagnetism, IEEE Press (1993).

[31] Stanford Reserach Systems, DSP lock-in amplifier, Model SR830 (2011)

[32] E. Paperno, IEEE Trans. Magn. VOL. 35 NO. 5 (1999)